Light-Induced Cytosolic Activation of Reduction-Sensitive Camptothecin-Loaded Polymeric Micelles for Spatiotemporally Controlled *in Vivo* Chemotherapy

Hung-Chi Yen,[†] Horacio Cabral,[†] Peng Mi,[‡] Kazuko Toh,[§] Yu Matsumoto,[§] Xueying Liu,[§] Hiroshi Koori,[∥] Ahram Kim,[†] Kozo Miyazaki,[§] Yutaka Miura,[§] Nobuhiro Nishiyama,[‡] and Kazunori Kataoka*[,†,§,⊥,#]

[†]Department of Bioengineering, Graduate School of Engineering, The University of Tokyo, 7-3-1 Hongo, Bunkyo-ku, Tokyo 113-8656, Japan, [‡]Polymer Chemistry Division, Chemical Resources Laboratory, Tokyo Institute of Technology, R1-11, 4259 Nagatsuta, Midori-ku, Yokohama 226-8503, Japan, [§]Division of Clinical Biotechnology, Center for Disease Biology and Integrative Medicine, Graduate School of Medicine, The University of Tokyo, 7-3-1 Hongo, Bunkyo-ku, Tokyo 113-0033, Japan, [∥]Pharmaceutical & Healthcare Research Laboratories, Research & Development Management Headquarters, Fujifilm Company, Ltd., 577 Ushijima, Kaiseimachi, Ashigarakami-gun, Kanagawa 258-8577, Japan, [⊥]Department of Materials Engineering, Graduate School of Engineering, The University of Tokyo, 7-3-1 Hongo, Bunkyo-ku, Tokyo 113-8656, Japan, and [#]Kawasaki Institute of Industry Promotion, 66-20 Horikawa-cho, Saiwai-ku, Kawasaki 212-0013, Japan

ABSTRACT Nanomedicines capable of smart operation at the targeted site have the potential to achieve the utmost therapeutic benefits. Providing nanomedicines that respond to endogenous stimuli with an additional external trigger may improve the spatiotemporal control of their functions, while avoiding drawbacks from their inherent tissue distribution. Herein, by exploiting the permeabilization of endosomes induced by photosensitizer agents upon light irradiation, we complemented the intracellular action of polymeric micelles incorporating camptothecin (CPT), which can sharply release the loaded drug in response to the reductive conditions of the cytosol, as an effective strategy for precisely controlling the function of these nanomedicines *in vivo*, while advancing toward a light-activated chemotherapy. These camptothecin-loaded micelles (CPT/m) were stable in the bloodstream, with minimal drug release in extracellular conditions, leading to prolonged blood circulation and high accumulation in xenografts of rat urothelial carcinoma. With the induction of endosomal permeabilization with the clinically approved photosensitizer, Photofrin, the CPT/m escaped from the endocytic vesicles of cancer cells into the cytosol, as confirmed both *in vitro* and *in vivo* by real-time confocal laser microscopies, accelerating the drug release from the micelles only in the irradiated tissues. This spatiotemporal switch significantly enhanced the *in vivo* antitumor efficacy of CPT/m without eliciting any toxicity, even at a dose 10-fold higher than the maximum tolerated dose of free CPT. Our results indicate the potential of reduction-sensitive drug-loaded polymeric micelles for developing safe chemotherapies after activation by remote triggers, such as light, which are capable of permeabilizing endosomal compartments.

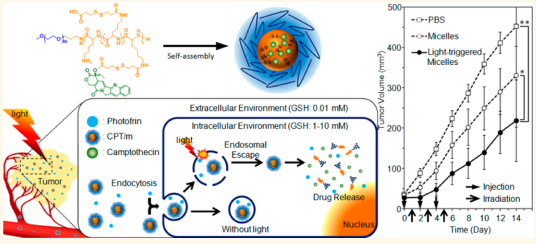

KEYWORDS: polymeric micelles · photochemical internalization · reduction-sensitive · camptothecin · glutathione · Photofrin

Nanomedicines with spatiotemporal control of their functions have the potential for the development of effective antitumor strategies with minimal side effects.[1−4] Particularly, nanomedicines responding to endogenous cellular stimuli have been considered for attaining selective intracellular delivery of drugs and maximizing therapeutic efficiency.[1−4] Endowing such nanomedicines with an additional external stimulus may provide further spatial and temporal control at the targeted position,[2,3] thereby, allowing precise operation at the aimed site, while eliminating detrimental issues rising from the distribution of nanomedicines to organs of the reticuloendothelial system.

Among exogenous stimuli, light has been considered as a safe and specific trigger for nanomedicines,[5,6] laser therapy,[7] and photodynamic therapy (PDT),[8] that is, the destruction of cancerous tissues *via* reactive

* Address correspondence to kataoka@bmw.t.u-tokyo.ac.jp.

Received for review August 28, 2014 and accepted October 21, 2014.

Published online October 21, 2014
10.1021/nn504836s

Scheme 1. Illustration of the photochemical internalization (PCI) activated chemotherapy using reduction-sensitive camptothecin (CPT)-loaded polymeric micelles (CPT/m)[a]

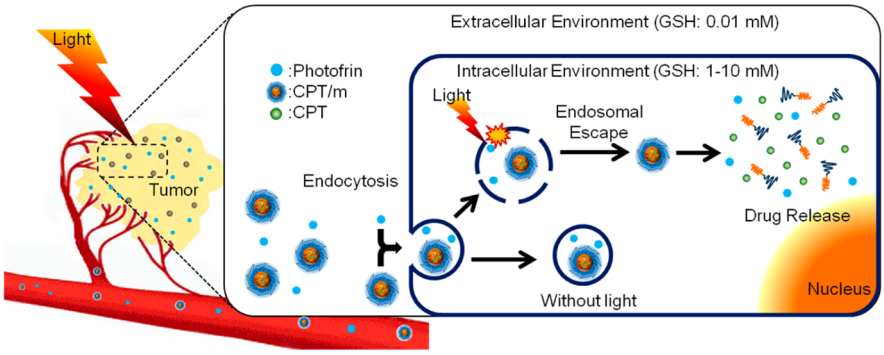

[a] CPT/m can prevent premature leakage of their cargo at extracellular conditions and preferentially accumulate in tumor tissue due to enhanced permeability and retention (EPR) effect. After light-irradiation, the membrane of endocytic vesicles are destabilized by reactive oxygen species (ROS) generated by photosensitizers (PS), *i.e.*, Photofrin, leading to endosomal escape of CPT/m and acceleration of drug release under cytosolic environment.

oxygen species produced by light-activated photosensitizer (PS) molecules is already used in the clinic. Moreover, the permeabilization of endosomal compartments by sublethal PDT has been recently used for enhancing the delivery of therapeutics[9] and nanomedicines[10−15] trapped in endosomal compartments into the cytosol upon light irradiation, so-called photochemical internalization (PCI). In this way, combination of PCI with endosomally internalized nanomedicines that specifically release their cargo in response to cytosolic conditions could be an effective approach for augmenting spatiotemporal control of their functions, and simultaneously evolve into applicable light-activated therapies.

Core−shell block copolymer micelles incorporating therapeutic agents in their cores have demonstrated outstanding features as nanomedicines in both preclinical and clinical studies,[16−18] including their adaptable drug release in response to specific stimuli by directly engineering the bond between the drugs and the core-forming segment of the block copolymers.[16−18] We have previously developed polymeric micelles exploiting disulfide bonds in their cores for specifically acting under the reductive conditions of the cytosol,[19−21] which shows 100- to 1000-fold higher glutathione (GSH) concentration than those in blood and extracellular milieu (Scheme 1).[22] As polymeric micelles enter cells *via* endocytosis and accumulate in endosomal/lysosomal compartments with insufficient redox-potential for thiol/disulfide exchange reaction,[23] micelle systems sensitive to reductive cytosolic environment could be effectively combined with PCI for controlling the position and timing of therapy after inducing their escape from endosomes into the cytosol.[21]

Herein, we report the first example of an *in vivo* light-activated chemotherapy combining systemically injected reduction-sensitive polymeric micelles and PCI. These micelles were self-assembled in water after conjugating the anticancer drug camptothecin (CPT) to the poly(L-lysine) block of poly(ethylene glycol)-poly(L-lysine) (PEG-P(Lys)) block copolymers *via* a disulfide linker. Moreover, Photofrin was selected as the PS due to its clinical relevance[24] and capability to induce PCI effect,[25] and the antitumor effects resulting from the PCI-mediated activation of the micelles were studied in a model of AY27 rat urothelial carcinoma because of the significant role of PDT and Photofrin against bladder cancer,[8,24] as well as the need for approaches capable of avoiding the typical damage of PDT to healthy bladder.[26] Our results proved that inducing the escape of the CPT-loaded micelles (CPT/m) from the endocytic vesicles into the cytosol accelerated their drug release only in the irradiated tissues (Scheme 1), which enhanced their antitumor efficacy without any toxicity, suggesting the potential of reduction-sensitive polymeric micelles for developing safe chemotherapies activated not only by PCI, but also by other external triggers capable of permeabilizing endosomal membranes.

RESULTS AND DISCUSSION

Preparation and Characterization of CPT-Loaded Micelles (CPT/m). PEG-P(Lys(TFA)) block copolymer was synthesized by ring-opening polymerization of lysine(TFA)-*N*-carboxyanhydride, as previously reported,[27] and showed a narrow molecular weight distribution (M_w/M_n = 1.04) as determined by gel permeation chromatography (GPC) (Supporting Information Figure S1). After the deprotection of TFA groups *via* alkali hydrolysis by 1N NaOH solution, the polymerization degree of the P(Lys) block was calculated to be 37 by comparing the proton peak ratio of methylene units of PEG with the β, γ, and δ-methylene protons of lysine in proton nuclear magnetic resonance (^{1}H NMR) spectrum (Supporting Information Figure S2). Then, thiolated PEG-P(Lys) block copolymer was prepared using

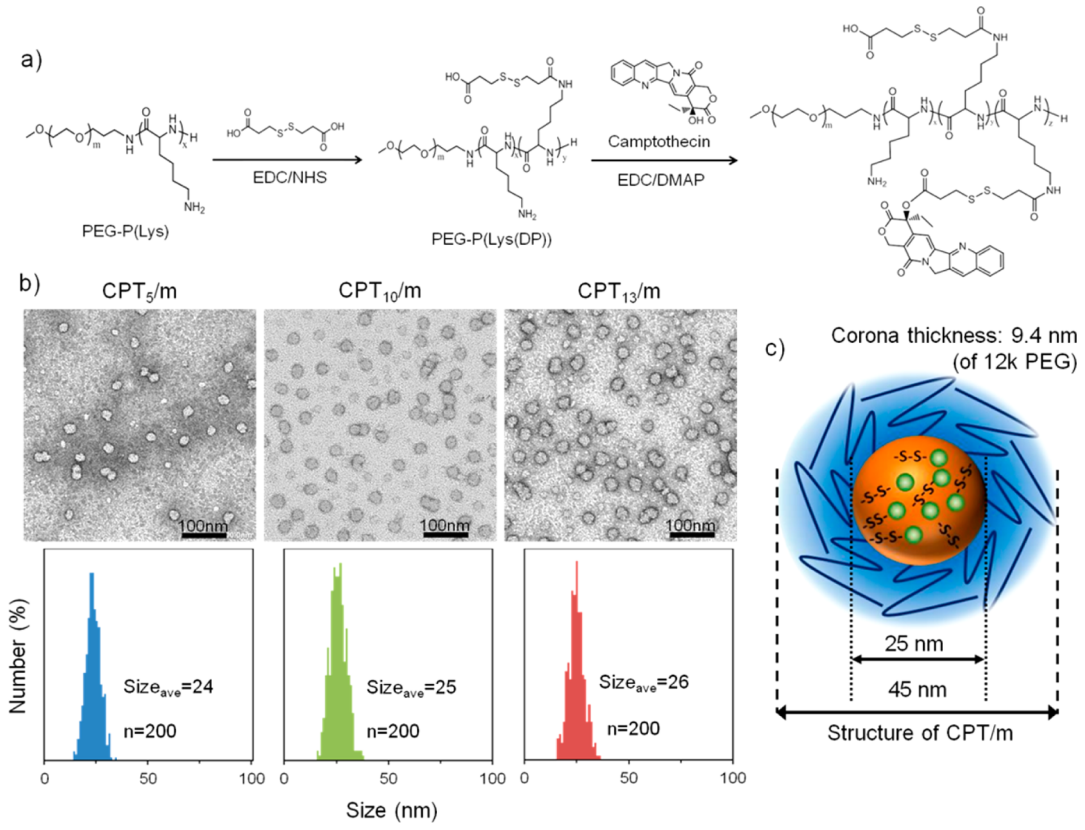

Figure 1. Preparation and characterization of CPT-loaded polymeric micelles (CPT/m). (a) Synthetic route of CPT/m. (b) TEM of CPT_5/m, CPT_{10}/m, and CPT_{13}/m stained with 2% uranyl acetate. Scale bar = 100 nm. The panels (bottom) are the number-based distribution histograms of the core diameter of the micelles calculated from the corresponding TEM images (n = 200). (c) Core-shell dimension of CPT/m, a hydrophobic core about 25 nm and a PEG shell around 9.4 nm.

TABLE 1. Characterization of CPT-Loaded Polymeric Micelles (CPT/m)

micelles	CPT feeding ([CPT]/[COOH])	Conjugation ratio ([CPT]/[COOH])[a]	CPT units per block copolymer	micelle loading (w/w %)	diameter (nm)[b]	PDI	core diameter (nm)[c]
CPT_5/m	1	0.16	5	7.50	43	0.15	24
CPT_{10}/m	2	0.31	10	13.1	44	0.17	25
CPT_{13}/m	5	0.40	13	16.3	45	0.16	26

[a] Determined by UV-vis spectrophotometer. [b] Number distribution determined by DLS. [c] Number distribution determined by TEM (n = 200).

1-ethyl-3-(3-(dimethylamino)propyl)carbodiimide (EDC) and *N*-hydroxysuccinimide (NHS) coupling reagents to conjugate 3,3′-dithiodipropionic acid with PEG-P(Lys) block copolymer (Figure 1a). The conjugation was confirmed by ^{1}H NMR by comparing the peaks of the methyl protons of conjugated 3,3′-dithiodipropionic acid with the proton peaks of free 3,3′-dithiodipropionic acid and a peak shift of the methylene protons adjacent to the amino group from 3.24 to 3.45 ppm (Supporting Information Figure S3). The conjugation ratio of 3,3′-dithiodipropionic acid to the amine groups was determined to be 87% by Ellman's test, indicating 32 units of 3,3′-dithiodipropionic acid on each block copolymer, and a minor fraction of polymer cross-link (4%) can be detected by GPC. The PEG-P(Lys(dithiopropionic acid)) block copolymer was then reacted with different amounts of CPT ([CPT]/[COOH] = 1, 2 or 5) by using EDC and 4-dimethylaminopyridine (DMAP) to form PEG-P(Lys(CPT)) block copolymer (Figure 1a).

CPT-conjugated block copolymers were then dissolved in DMSO and dialyzed against water to self-assemble into CPT/m. The hydrodynamic size of the micelles having different CPT loading was found to be comparable among the formulations, that is, approximately 45 nm with a relatively narrow polydispersity index (PDI), as determined by dynamic light scattering (DLS) (Table 1). The morphology of the micelles was further studied by transmission electron microscopy (TEM) after negative staining with uranyl acetate. Because the PEG shell of micelles is not detectable in micelles stained by uranyl acetate, the TEM observations allowed us to measure of the diameter of the core of CPT/m, which was determined to be approximately 25 nm (Figure 1b). The resulting size distributions from

DLS and TEM suggest that CPT/m were 45 nm with a hydrophobic core of approximately 25 nm (Figure 1c) and a calculated corona thickness of 9.4 nm, which appropriately correlates with the previously reported squeezed conformation of PEG chain of long-circulating micelles using 12 kDa PEG.[28−30] Besides the thick PEG shell of micelles, the surface charge of CPT/m determined as ζ-potential at pH 7.4 was found to be close to neutral (+0.26 mV), which is a significant advantage for avoiding the adsorption of charged biomolecules and extending the half-life in the bloodstream.[16−18,31]

The loading of CPT in the micelles was controlled from 7.50 to 16.3 w/w % (weight of drug/weight of polymer: w/w) (Table 1), as determined by UV-vis spectrophotometer. By increasing the [CPT]/[COOH] feed ratio from 1 to 2, the loading of the micelles was practically doubled (Table 1). However, increasing this feed ratio from 2 to 5 slightly augmented the loading of the micelles from 13.1 to 16.3 w/w %, probably due to steric hindrance of the polymer-conjugated CPT, decreasing the loading efficiency of the micelles (Table 1). Because these CPT molecules are loaded *via* a disulfide linkage, CPT/m may allow the selective release of the loaded drugs in the cytosolic environment.

Drug Release from CPT-Loaded Micelles (CPT/m). The CPT release from CPT/m was studied under various conditions to verify the sensitivity of the micelles to reductive conditions. First, as dithiothreitol (DTT) is a common agent used in the literature for reducing disulfide bonds in reduction-sensitive drug carriers, we studied the drug release of our micelles with different CPT loading, *i.e.*, CPT/m having 5 CPT molecules (CPT_5/m), 10 CPT molecules (CPT_{10}/m), and 13 CPT molecules per block copolymer (CPT_{13}/m), by exposing them to 10 mM dithiothreitol (DTT) in PBS buffer at pH 7.4. Under this condition, we observed an accelerated CPT release from all micelles reaching more than 90% within 2 h (Figure 2a). Interestingly, the release rate of CPT from CPT/m revealed a loading dependent delay in the first 2 h, which may be attributed to the increased hydrophobicity of the core of CPT/m, resulting in a retarded degradation rate of the disulfide bonds and a slower diffusion of the loaded CPT molecules toward the media. On the other hand, in PBS buffer at physiological pH (pH 7.4) or at endosomal pH (pH 5.5) without DTT, CPT_{10}/m showed less than 3% of drug released after 4 h incubation, indicating the specificity of CPT/m for discharging the drug at reductive conditions. Because of this selective release at reductive conditions of CPT_{10}/m, as well as their high and efficient CPT loading, these micelles were selected for further study of their *in vitro* and *in vivo* properties.

In addition, as glutathione (GSH) is the major reductive molecule in the cytosol,[22] the release rate of CPT_{10}/m was studied under GSH concentrations simulating cytosolic (1−10 mM) and extracellular (0.01 mM) conditions (Figure 2b). Thus, at 5−10 mM of GSH, the

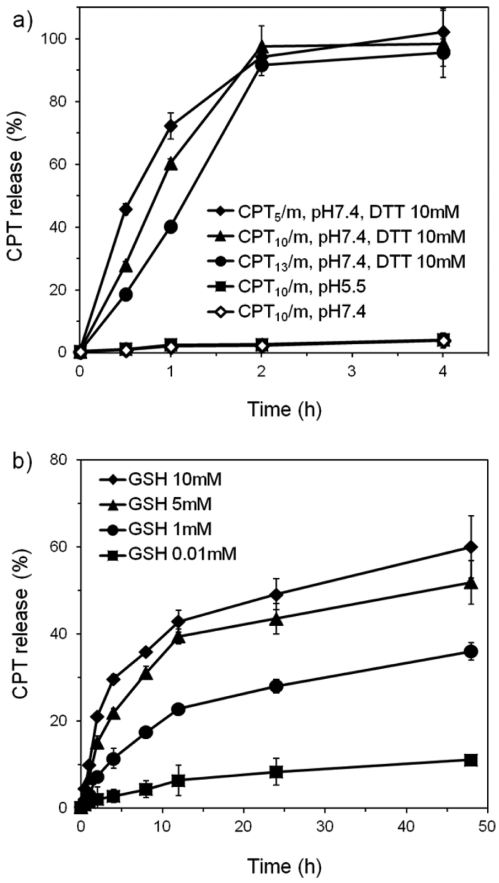

Figure 2. Drug release profiles of CPT-loaded micelles (CPT/m) under conditions simulating different physiological environments. (a) Percentage of CPT release from CPT/m with different CPT-loading in PBS buffer at pH 7.4 using dithiothreitol (DTT) as reducing agent, and at physiological pH (pH 7.4) or at endosomal pH (pH 5.5) without DTT. (b) Percentage of CPT release of CPT_{10}/m in PBS buffer at pH 7.4 containing different concentration of glutathione (GSH) simulating extracellular and cytosolic conditions. The results represent average values ± SD (n = 3).

percentage of drug release was found to be approximately 50% after 24 h, which was 10-fold higher than the CPT released in 0.01 mM of GSH. This rapid and preferential drug release of CPT_{10}/m under cytosolic conditions could be employed for selective PCI-mediated intracellular delivery of CPT in cancer cells.

Enhancement of Cytotoxicity of CPT-Loaded Micelles (CPT/m) by Photochemical Internalization (PCI). The viability of AY27 rat bladder cancer cells after incubation with free CPT and CPT_{10}/m was studied to determine the cytotoxic effect with or without PCI. Both drugs were combined with 0.1 μg/mL Photofrin, which were found to be non-cytotoxic after irradiation (fluence rate, 3.0 mW/cm^2; time, 10 min) (Supporting Information Figure S4). Without light irradiation, free CPT showed approximately 100-fold lower 50% inhibitory concentration (IC_{50}) than CPT_{10}/m (Table 2). Moreover, the cytotoxicity of free CPT plus Photofrin was not modified by light irradiation (Table 2), while the thiolated CPT showed similar *in vitro* cytotoxicity to free CPT (Supporting

Information Figure S5). Conversely, 10 min irradiation of CPT_{10}/m plus 0.1 μg/mL Photofrin enhanced the cytotoxicity of the micelles, showing more than 3-fold decrease in the IC_{50} compared to the nonirradiated sample (Table 2). Even 0.01 μg/mL Photofrin and 10 min irradiation induced the enhancement of *in vitro* cytotoxicity of CPT_{10}/m, suggesting the capability of Photofrin for improving the efficacy of these reduction-sensitive micelles. This enhancement of the cytotoxicity of CPT_{10}/m could be attributed to the photoinduced permeabilization of endocytic membranes by the generated ROS species from Photofrin after light exposure, followed by the endosomal escape of micelles and the accelerated release of CPT.

TABLE 2. Cytotoxicity of Free CPT and CPT-Loaded Micelles (CPT/m) with Photofrin against AY27 Urothelial Carcinoma

		IC50 (μM)[a]		
drug	photofrin (μg/mL)	nonirradiated	irradiated[b]	nonirradiated/ irradiated ratio
Free CPT	0	0.06 ± 0.01	-	-
Free CPT	0.1	-	0.06 ± 0.01	1
CPT_{10}/m	0	5.70 ± 0.29	-	-
CPT_{10}/m	0.01	-	2.70 ± 0.33	2.11
CPT_{10}/m	0.1	-	1.90 ± 0.19	3.03

[a] Determined by WST-8 assay (n = 4). [b] cells were irradiated for 10 min.

***In Vitro* Microscopic Evaluation of the Photochemical Internalization (PCI) of CPT-Loaded Micelles (CPT/m).** The capability of Photofrin to induced endosomal escape of CPT/m by PCI was evaluated by following the time-dependent intracellular distribution of CPT_{10}/m labeled with Alexa 555 in AY27 cells *via* confocal laser scanning microscopy (CLSM). The late endosomes of AY27 cells were initially marked using CellLight Late Endosomes-GFP (green). These cells were incubated with Alexa 555-labeled CPT_{10}/m (red) and Photofrin for 24 h. At this time-point, the signal of micelles was colocalized with that of late endosomes (Figure 3a; yellow). Then, the cells were irradiated with the same light dose as the *in vitro* cytotoxicity experiment (3.0 mW/cm^2, time: 10 min), and the escape of the micelles from the late endosomes was followed by assessing the CPT/m/endosomes colocalization ratio. After 120 min, the endosomal escape of Alexa 555-labeled CPT_{10}/m (Figure 3a; red) in irradiated cells was evident, whereas the cells without light irradiation (Figure 3a; yellow) and the cells only treated with light (Supporting Information Figure S7) maintained the level of colocalization of micelles with late endosomes. Moreover, the colocalization ratio of micelles and late endosomes in irradiated AY27 cells was significantly reduced from 70% at 0 h to 55% at 21 h after irradiation (Figure 3b; $p < 0.01$). Thus, this PCI-triggered translocation of CPT/m from endosomal compartments into the reductive cytosol may result in the enhanced intracellular

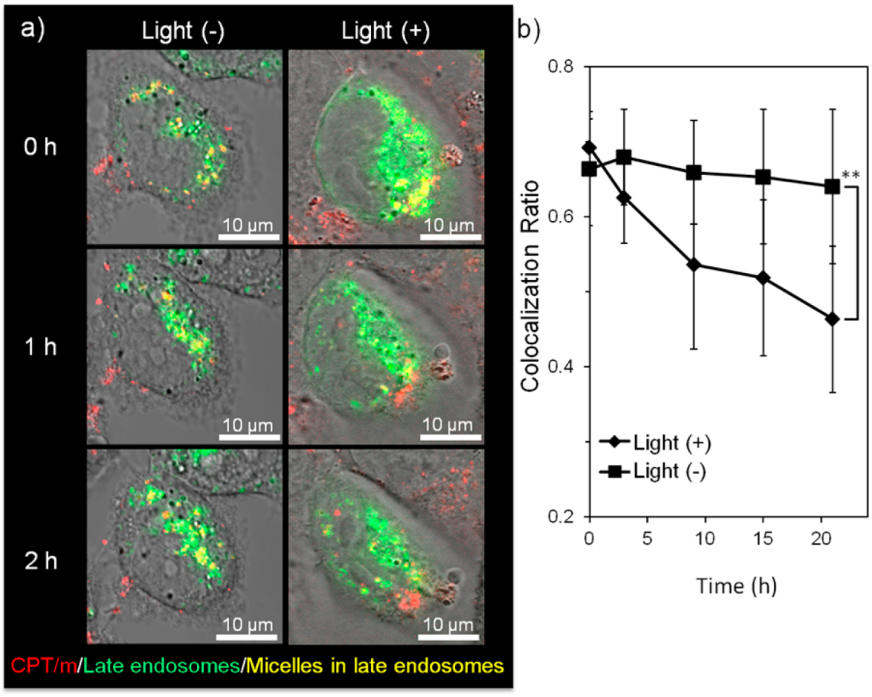

Figure 3. ***In vitro*** **real-time microscopic evaluation of the photochemical internalization (PCI) of CPT/m induced by Photofrin. (a)** ***In vitro*** **CLSM images of time-dependent intracellular distribution of Alexa 555-labeled CPT_{10}/m (red) in AY27 cells prelabeled with CellLight Late Endosomes-GFP (green). After irradiation (3.0 mW/cm^2, time: 10 min), the AY27 cells treated with Photofrin showed a capability of endosomal escape. CLSM images were taken at 0, 60, and 120 min postirradiation. Scale bar = 10 μm. (b) Colocalization ratio of Alexa 555-labeled CPT_{10}/m with late endosomes in AY27 cells quantified using Imaris software. The results represent average values ± SD (n = 30), $^{**}p < 0.01$.**

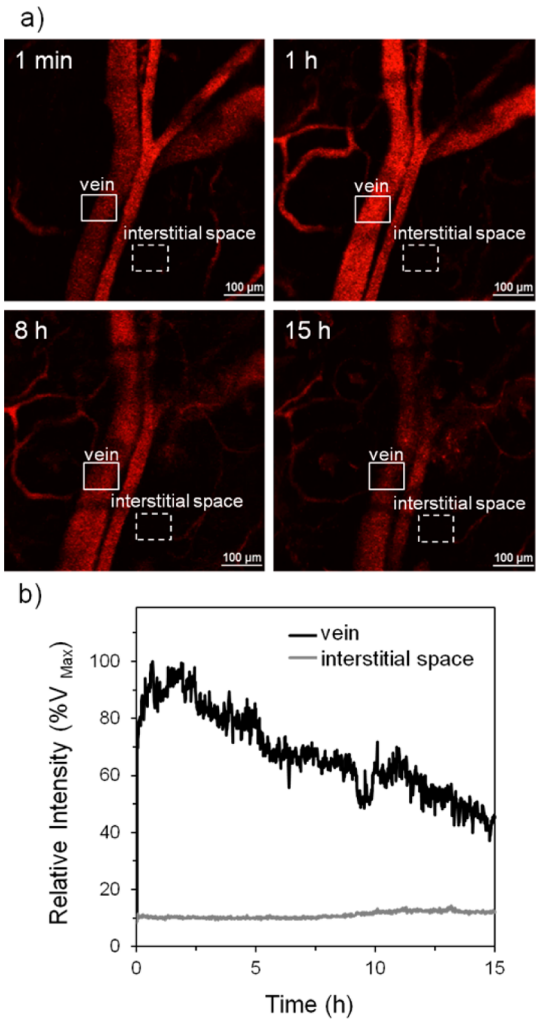

Figure 4. Blood circulation of CPT-loaded micelles (CPT/m) and Photofrin assessed by intravital real-time confocal laser scanning microscopy (IVRTCLSM). (a) Snap-shots of mouse ear-lobe 1 min, 1, 8, and 15 h after the iv injection of Alexa 555-labeled CPT_{10}/m (red). Scale bar = 100 μm. (b) Time-dependent *in vivo* fluorescence intensity of micelles in the selected regions of vein (square) and interstitial space (dotted square) expressed as the percentage of maximum fluorescence intensity achieved in the vein (%V_{max}).

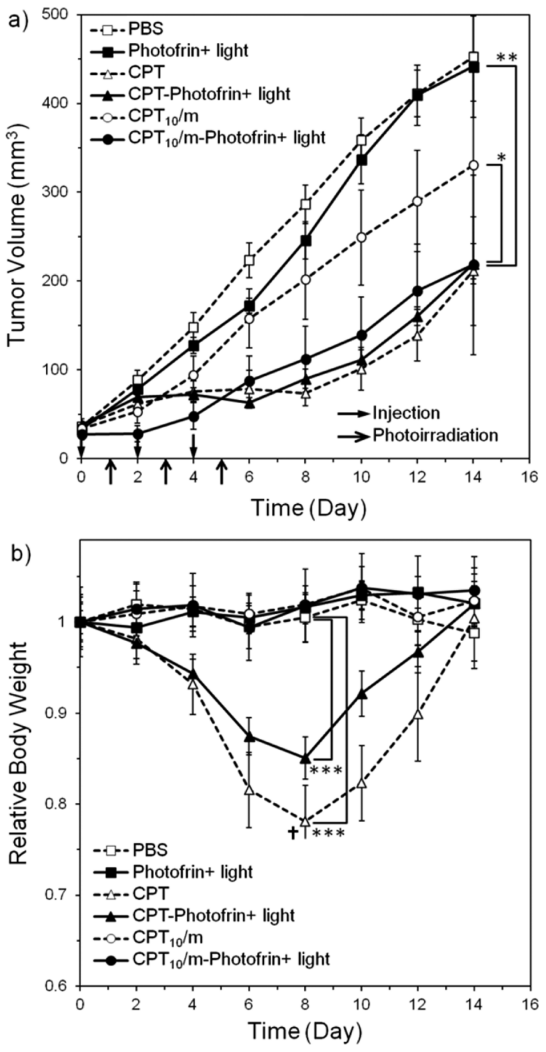

Figure 5. Antitumor activity of CPT-loaded micelles (CPT/m) with or without Photofrin induced photochemical internalization (PCI) against AY27 subcutaneous xenografts ($n = 4$). (a) Tumor volume (mm^3) after treatment with PBS (□), Photofrin at 2 mg/kg (■), CPT at 5 mg/kg (Δ), CPT at 5 mg/kg with Photofrin at 2 mg/kg (▲), CPT_{10}/m at 50 mg/kg (○), and CPT_{10}/m at 50 mg/kg with Photofrin at 2 mg/kg (●). The treated light intensity was 100 mW/cm^2 (time: 1000 s). The results represent as average values ± SD, *$p < 0.05$, **$p < 0.01$. (b) Relative body weight of mice after treatment with PBS (□), Photofrin at 2 mg/kg (■), CPT at 5 mg/kg (Δ), CPT at 5 mg/kg with Photofrin (▲), CPT_{10}/m at 50 mg/kg (○), and CPT/m at 50 mg/kg with Photofrin (●). †: 1/5 mice toxic death. The results represent average values ± SD, ***$p < 0.001$.

release of CPT, which could be a substantial advantage for developing safe and tumor-specific cytotoxic therapies.

Blood Circulation of CPT-Loaded Micelles (CPT/m). For effectively exploiting the selective tumor accumulation through the enhanced permeability and retention (EPR) effect,[32] *i.e.*, the facilitated penetration of macromolecules through the leaky vasculature of tumors and the retention of these macromolecules due to the impaired lymphatic drainage in these tumors, CPT/m should stably circulate in the bloodstream for prolonged time. Therefore, we assessed the circulation time of CPT_{10}/m in the bloodstream by using intravital real-time confocal laser scanning microscopy (IVRTCLSM), which can allow real-time noninvasive and quantitative evaluation of *in vivo* dynamic processes of polymeric micelles.[33] Thus, the fluorescence intensities of Alexa 555-labeled CPT_{10}/m (red) in the blood vessels of the ear-lobe, as well as in the interstitial space, were followed for up to 15 h. Snap-shots at 1 min, 1, 8, and 15 h post iv injection of the micelles (Figure 4a) and the fluorescence intensity profile in the blood vessels (Figure 4b) revealed that the Alexa 555-labeled CPT_{10}/m have prolonged circulation in the bloodstream for more than 15 h (Figure 4b). Moreover, CPT/m did not extravasate into the interstitial space of the ear lobe, indicating that the micelles did not dissociate into the forming block copolymers during

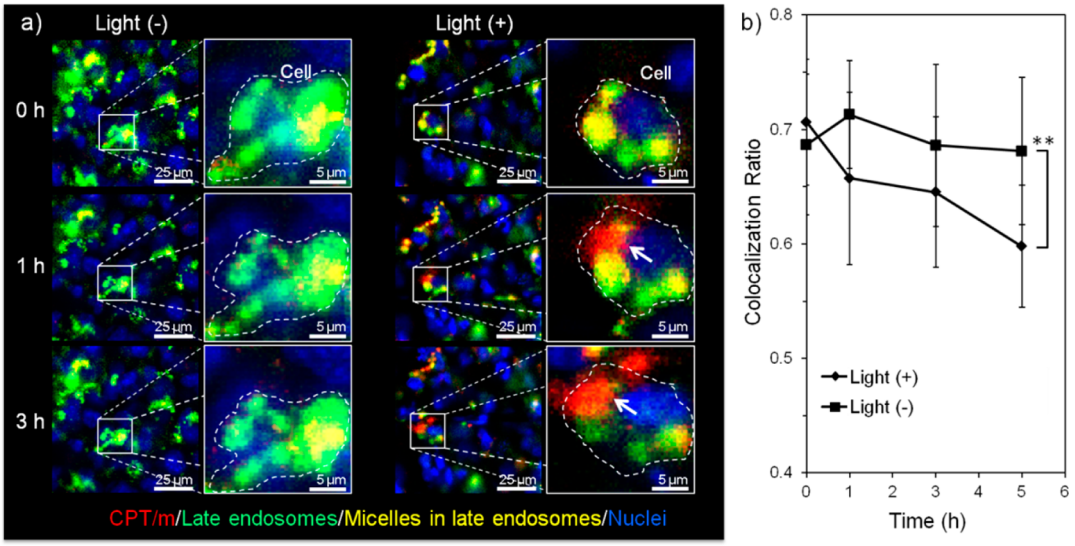

Figure 6. ***In vivo*** **real-time CLSM evaluation of Photofrin-induced photochemical internalization (PCI) of CPT-loaded micelles (CPT/m). (a)** ***In vivo*** **time-dependent intracellular distribution of Alexa 555-labeled CPT/m (red) in the cells of a AY27 xenograft prelabeled with CellLight Late Endosomes-GFP (green). The snapshots were obtained at 0, 1, and 3 h after light irradiation (fluence rate, 100 mW/cm^2; time, 20 s). Left column are nonirradiated tumors (light (−)), and right column are irradiated tumors (light (+)). The arrows indicate the gradual escape of micelles from late endosomes. (b) Time-dependent change of colocalization ratio of CPT/m with late endosomes quantified using Imaris software. The results represent average values ± SD (*n* = 20), **$p < 0.01$.**

blood circulation. In addition, the blood circulation of Photofrin after iv injection was also evaluated (Supporting Information Figure S8). Contrary to CPT/m, Photofrin was observed in the interstitial space of healthy skin tissue 8 h after injection (Supporting Information Figure S8), which can be associated with its skin phototoxicity reported in the clinic.[24] It is worth mentioning that, even though the PS molecules accumulate in healthy tissue, the strategy proposed in this study can overcome such drawback as the extravasation and accumulation of CTP/m in healthy tissue is minimal (Figure 4a,b) and the PS doses required for PCI are nontoxic, which may result in safe light-activated chemotherapies.

In Vivo **Antitumor Activity of CPT-Loaded Micelles (CPT/m).** Twenty-four hours after iv injection, the amount of CPT delivered by CPT_{10}/m in subcutaneous AY27 xenografts was determined to be 11 ± 1.52% of the injected dose per gram of tissue. Moreover, the CPT levels were maintained 48 h after iv administration of the micelles (13 ± 1.95% of the injected dose per gram of tissue). This elevated concentration of CPT/m in tumor tissue is comparable to that achieved by other long-circulating micelles accumulating in solid tumors *via* the EPR effect,[30,34−36] and may be advantageous for accomplishing the high antitumor efficacy.

The effect of Photofrin-induced PCI on the *in vivo* antitumor activity of CPT/m was evaluated in nude mice bearing subcutaneous AY27 xenografts (*n* = 4). Mice treated with 3 iv injections every second day, *i.e.*, on days 0, 2 and 4, of Photofrin at 2 mg/kg followed by irradiation (100 mW/cm^2; time, 1000 s) on days 1, 3, and 5 (Figure 5a; Photofrin + light) showed comparable tumor growth to mice receiving PBS injections (Figure 5a; PBS), indicating that Photofrin at this dosage does not afford significant antitumor effect. Thus, this Photofrin dosing was used in combination with free CPT at its maximum tolerated dose, that is, 5 mg/kg, or CPT_{10}/m at 50 mg/kg on a CPT base, which were intravenously injected following the same schedule as Photofrin, for determining the enhancement of the antitumor efficacy after PCI. The activity of free CPT at 5 mg/kg was not affected by the induction of PCI by Photofrin (Figure 5a; CPT and CPT-Photofrin + light), as free CPT enters cells by diffusion.[37] Conversely, while CPT_{10}/m at 50 mg/kg showed moderate antitumor effect (Figure 5a; CPT_{10}/m), the application of PCI significantly enhanced the activity of the micelles (Figure 5a; CPT_{10}/m -Photofrin + light) compared to PBS ($p < 0.01$) and CPT_{10}/m at 50 mg/kg groups ($p < 0.05$). Also, it is worth noting that, while free CPT at 5 mg/kg caused considerable loss of the body weight of mice (Figure 5b; $p < 0.001$), and 1 out of 5 mice died at day 8 in the free CPT plus PCI group due to toxicity, the weight of mice treated with CPT_{10}/m at 50 mg/kg was not affected during the antitumor activity experiment (Figure 5b), most likely due to the site-specific control of the micelles by PCI, and the controlled release of CPT from the micelles under cytosolic conditions.

In Vivo **Real-Time CLSM Analysis of the Photochemical Internalization (PCI) of CPT-Loaded Micelles (CPT/m).** To confirm that Photofrin induced PCI of CPT/m *in vivo*, the intracellular distribution of Alexa 555-labeled CPT_{10}/m in AY27 xenografts in a living mouse was analyzed by *in vivo* CLSM. Initially, a subcutaneous AY27 tumor was

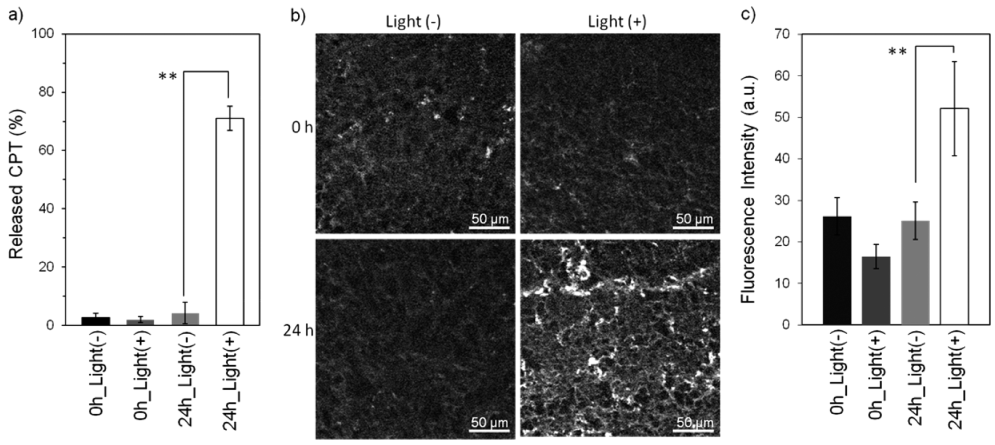

Figure 7. ***In vivo*** **enhancement of drug release from CPT-loaded micelles (CPT/m) after photochemical internalization (PCI). (a) PCI enhanced drug release of CPT from CPT/m in AY27 subcutaneous xenografts at 0 and 24 h postirradiation. The values represent average values ± SD (*n* = 4), ***p* < 0.01. (b) Distribution of CPT (white) from CPT/m determine by CLSM of sections of AY27 tumors with (light(+)) or without PCI (light(−)). CPT becomes detectable after release from CPT/m, while inside the micelles, CPT is quenched. Scale bar = 50 μm. (c) Mean fluorescence intensity of CPT quantified from the CLSM images with or without light-exposure (*n* = 30), ***p* < 0.01.**

surgically exposed, and the late endosomes in the cells of the tumor were marked by dropping 10 μL of CellLight Late Endosomes-GFP (green) on the xenograft. Twenty-four hours later, Photofrin at 2 mg/kg and the fluorescent micelles were intravenously injected. After 24 h, the micelles (red) were visualized in the late endosomes (green) of the cells in the tumor (Figure 6a; yellow). In addition, Hoechst 33342 was used to stain the nucleus of AY27 cells to distinguish the position of single cells (Figure 6a; blue). After treatment with light irradiation (fluence rate, 100 mW/cm^2; time, 20 s), the signal from CPT/m (red) gradually separated from that of late endosomes (green), indicating the endosomal escape of the micelles (Figure 6a; light (+)). Conversely, in a nonirradiated tumor, the colocalization of the micelles and late endosomes (yellow) was observed throughout the experiment (Figure 6a; light (−)). Moreover, the colocalization ratio of micelles and late endosomes was reduced from 70% to 59% 5 h after irradiation (Figure 6b). To our knowledge, this is the first report showing in real-time the escape of nanomedicines from endosomal compartments after PCI *in vivo*, which not only allowed us to confirm the design of our strategy by direct visualization of the process, but could also serve for expanding the insights of the intracellular processes for other nanomedicines and therapeutics after the application of triggers permeabilizing endosomal membranes *in situ*. The facilitated access of CPT/m to the cytosol after PCI, observed in these intravital microscopies, may promote the drug release from the micelles within the tumors, improving their therapeutic efficiency.

In Vivo **Enhancement of Drug Release from CPT-Loaded micelles (CPT/m) after Photochemical Internalization (PCI).** Twenty-four hours after co-injection of CPT_{10}/m and Photofrin, the tumors were irradiated (fluence rate, 100 mW/cm^2; time, 1000 s) to induce the PCI effect. Then, the PCI-induced release of CPT from CPT_{10}/m within AY27 tumors was assessed by calculating the amount of free CPT at 0 and 24 h after irradiation obtained by reverse phase liquid chromatography (RPLC) of homogenized tumor tissues. The homogenized samples were divided into two parts, one part was treated with DTT to determine the total CPT amount in the tumor, which was considered as 100%, and the other part was directly evaluated by RPLC for detecting the released CPT. Thus, while the release of CPT from the micelles within tumors without irradiation was less than 4%, the drug release increased more than 70% from 0 to 24 h after irradiation (Figure 7a). This significant increment of CPT release was further demonstrated by studying the fluorescence of CPT in tumor sections by using CLSM (Figure 7b and 7c). Accordingly, after PCI, the fluorescence signal from CPT in tumor tissues augmented due to the release and dequenching of the CPT molecules that were loaded in the core of CPT/m (Supporting Information Figure S9), whereas in nonirradiated tumor tissues CPT molecules remained quenched in the cores of micelles (Figure 7b,c). These results support the enhancement of the *in vivo* antitumor activity of CPT/m after the application of PCI (Figure 5a), and denote the ability of reduction-sensitive drug-loaded polymeric micelles for developing safe and site-specific chemotherapies activated by PCI. In addition, the combination of this strategy with whole bladder wall photodynamic therapy[38,39] may result in safe and efficient treatments without damaging to healthy bladder tissues. Moreover, other external stimuli capable of permeabilizing endosomal membranes, such as photothermal,[40] ultrasound,[41] or magnetic triggers,[42] could be potentially combined with polymeric micelles releasing their payloads in response to cytosolic signals for designing highly selective antitumor treatments.

CONCLUSION

In this study, we developed reduction-sensitive polymeric micelles for selectively releasing CPT loaded in their core under cytosolic conditions, and showed that the function of these micelles can be remotely controlled after promoting their escape from endosomal compartments in cells within tumors by PCI, to exert strong inhibition of the tumor growth without toxicity. These results demonstrate the capability of spatiotemporal control of the cytosolic activation of reduction-sensitive micelles for developing safe and effective therapies, and suggest the potential of modulating biological events within diseased tissues by using exogenous triggers for amplifying the activity of nanomedicines. As the light source can be coupled to optical fiber technologies, mucosal cancer or deep tumors could be readily accessed for achieving effective light-activated treatments. Furthermore, as a broad variety of therapeutic agents can be incorporated inside polymeric micelles, the design of reduction-sensitive micelles can be readily tailored to fulfill therapeutic requirements and facilitate the development of remotely activated therapies with potential for clinical translation.

MATERIALS AND METHODS

Materials. α-Methoxy-ω-aminopoly(ethylene glycol) (MeO-PEG-NH_2; M_w = 12 000) was purchased from NOF Corporation. (Tokyo, Japan). ε-Trifluoroacetyl-L-lysine *N*-carboxyanhydride (Lys(TFA)-NCA) was prepared by Fuchs-Farthing method using triphosgene as previously reported.[43] Dichloromethane (CH_2Cl_2), *N*,*N*-dimethylformamide (DMF), dimethyl sulfoxide (DMSO), and triethylamine (TEA) were purchased from Wako Pure Chemical Industries (Osaka, Japan). All the solvents were dried by general method before use. Bis(trichloromethyl)-carbonate (Triphosgene), methanol (MeOH), 3,3′-dithiodipropionic acid, 1-ethyl-3-(3-(dimethylamino)propyl)carbodiimide hydrochloride (EDC), *N*-hydroxysuccinimide (NHS), 4-dimethylaminopyridine (DMAP), camptothecin (CPT), dithiothreitol (DTT), and glutathione reduced form (GSH) were purchased from Tokyo Chemical Industry Co., Ltd. (Tokyo, Japan). 5,-5′-Dithio-bis(2-nitrobenzoic acid) (Ellman's reagent) was purchased from Thermo Scientific Co., Ltd. (Waltham, MA). Photofrin was purchased from Takeda Pharmaceutical (Osaka, Japan). Alexa Fluor 555-succinimidyl ester, Hoechst 33342, and CellLight Late Endosomes-GFP were purchased from Life Technologies Japan Co., Ltd. (Tokyo, Japan). AY27 cells were kindly provided by Dr. S. Sato, National Defense Medical College, Saitama, Japan.

Synthesis and Characterization of PEG-P(Lys) Block Copolymer. PEG-poly(L-lysine) (PEG-P(Lys)) block copolymer was synthesized by ring-opening polymerization of Lys(TFA)-NCA, and subsequently deprotection of trifluoroacetyl groups.[26] Briefly, Lys(TFA)-NCA (576 mg; 2.15 mmol) dissolved in anhydrous DMF was added to the solution of MeO-PEG-NH_2 (600 mg; 0.05 mmol). The mixture was stirred for 48 h at 35 °C under Ar atmosphere. The polymer was obtained by precipitation in diethyl ether three times and dried by vacuum. The molecular weight distribution of the obtained PEG-P(Lys(TFA)) block copolymer was characterized by gel permeation chromatography (GPC) (columns, TSK-gel G3000HHR, G4000HHR (Tosoh, Tokyo, Japan); eluent, DMF, containing 10 mM LiCl, 40 °C; flow rate, 0.8 mL/min; detector, refractive index). To remove the protective trifluoroacetyl (TFA) groups, PEG-P(Lys(TFA)) was dissolved in methanol solution containing 1 N NaOH to react for 6 h at 35 °C, and purified by dialysis against methanol (molecular weight cutoff (MWCO): 12 000−14 000). Finally, PEG-P(Lys) block copolymer was obtained by lyophilization. The polymerization degree of PEG-P(Lys) was determined by ^{1}H NMR by comparing the proton peak ratio of methylene units of PEG (−$C\underline{H}_2C\underline{H}_2$O−: δ = 3.7 ppm) with the β, γ, and δ-methylene protons of lysine ($C\underline{H}_2C\underline{H}_2C\underline{H}_2$, δ = 1.3−1.9 ppm) in ^{1}H NMR spectrum.

Synthesis and Characterization of Thiolated PEG-P(Lys). 3,3′-Dithiodipropionic acid (20 equiv of carboxyl groups to the amino groups of lysine, 1346 mg, 6.4 mmol,) was dissolved in DMF (5 mL), while EDC (8 equiv, 982 mg, 5.12 mmol) and NHS (8 equiv, 626 mg, 5.12 mmol) were dissolved in CH_2Cl_2 (5 mL). Then, the two solutions were mixed with stirring for 30 min to generate the EDC-activated carboxylic derivative. Meanwhile, PEG-P(Lys) block copolymer (300 mg, 0.016 mmol) was dissolved in DMF (10 mL) containing TEA, and added to the 3,3′-dithiodipropionic acid solution dropwisely to react for 24 h with stirring at room temperature. The thiolated PEG-P(Lys) (PEG-P(Lys(DP))) block copolymer was obtained by dialysis against water and lyophilization. The conjugated units was confirmed by ^{1}H NMR spectrum from the peaks of the methyl protons of 3,3′-dithiodipropionic acid (−COC$\underline{H}_2C\underline{H}_2SSC\underline{H}_2C\underline{H}_2$COOH, δ = 2.86−3.04 ppm), and the conjugation ratio of 3,3′-dithiodipropionic acid was quantified by Ellman's test.[44]

Preparation and Characterization of Camptothecin-Loaded Polymeric Micelles (CPT/m). PEG-P(Lys(DP)) block copolymer (300 mg, 0.012 mmol) dissolved in DMF (10 mL) was mixed with EDC (368 mg, 1.92 mmol) and DMAP (235 mg, 1.92 mmol) solution in CH_2Cl_2. The mixture was stirred for 30 min at room temperature, and then CPT dissolved in DMF was added at different concentrations (1, 2, and 5 equiv to carboxylic acid groups of P(Lys(DP)) to react for 24 h at room temperature with stirring in dark environment. The CPT-polymer conjugate was subsequently dialyzed against DMSO and methanol (MWCO: 12 000−14 000). When changing the dialysate to water, the drug-polymer conjugate self-assembled into CPT/m. Then, the micelle solution was further purified by ultrafiltration (MWCO: 30 000) and 0.22-μm syringe filters. The size distribution of CPT/m was evaluated by dynamic light scattering (DLS) measurement using a Zetasizer Nano ZS (Malvern Instruments Ltd., Worcestershire, United Kingdom). The CPT/m was stained with uranyl acetate and the morphology was observed using a transmission electron microscopy (TEM, JEM-1400, JEOL Co., Ltd., Tokyo, Japan) operated at an acceleration voltage of 100 kV. The number-average diameter of CPT/m was measured by ImageJ software according to the TEM images. The CPT concentration of CPT/m was determined by UV−vis spectrophotometer (V-550, JASCO Co., Ltd., Tokyo, Japan). Fluorescent-labeled micelles were prepared by labeling Alexa 555-succinimidyl ester to CPT-polymer conjugate and stirred for 24 h at room temperature in dark condition. The Alexa 555-labeled CPT-polymer conjugates were purified by gel filtration chromatography with a Sephadex LH-20 (GE Healthcare, Little Chalfont, United Kingdom) column using DMSO as eluent.

Drug Release Rate of CPT/m under Different Conditions. The release rate of CPT from the CPT/m was evaluated by dialysis method (MWCO: 3500) under different conditions. Briefly, CPT/m were dialyzed at 37 °C in physiological conditions of 10 mM phosphate buffer containing 150 mM NaCl (PBS) at normal pH (pH 7.4) and endosomal pH (pH 5.5), PBS buffer (pH 7.4) containing 10 mM dithiothreitol (DTT), and PBS buffer (pH 7.4) having glutathione at different concentrations (GSH; 0.01, 1, 5, and 10 mM). The solution outside of the dialysis bag was sampled at fixed time point and the concentration of CPT was evaluated using fluorescence spectrometer (FP-6500, JASCO Co., Ltd., Tokyo, Japan).

***In Vitro* Cytotoxicity Assay.** The *in vitro* cytotoxicity was determined by evaluating the 50% inhibitory concentration (IC_{50}) against AY27 rat bladder cancer cells according to the results of water-soluble tetrazolium salts (WSTs) assay using WST-8. AY27

cells (3000 cells/well) were seeded into 96-well plates in 50 μL of RPMI-1640 medium supplemented with 10% FBS. At first, the nontoxic concentration range of Photofrin for PCI effect against AY27 cancer cells was determined, and the detailed procedure is supplemented in Supporting Information (Figure S4). Next, the cancer cells were exposed to free CPT or CPT/m plus a nontoxic concentration of Photofrin for 24 h, followed by light irradiation (fluence rate, 3.0 mW/cm^2; time, 10 min) using a 300 W halogen lamp box equipped with a band-pass filter (400 nm-700 nm). Then, the irradiated cells were incubated for another 24 h, and the cell viability was evaluated with WSTs assay and measured the absorbance at 450 nm.

***In Vitro* Confocal Laser Scanning Microscopic (CLSM) Observation.** For studying the PCI-induced endosomal escape of CPT/m, LSM 780 (Carl Zeiss, Oberkochen, Germany), equipped with a 63× objective C-Apochromat (Carl Zeiss, Oberkochen, Germany), was used for the observation. AY27 cells (2×10^4 cells) were seeded on a 24 mm glass based dish (Iwaki Co., Ltd., Tokyo, Japan), and the late endosomes were marked with CellLight Late Endosomes-GFP. The cells were then treated with Alexa 555-labeled CPT/m plus a nontoxic concentration Photofrin (0.1 μg/mL). Twenty-four hours later, the cells were washed with PBS three times and replaced with fresh medium. Then, the cancer cells were irradiated (fluence rate, 3.0 mW/cm^2; time:, 10 min) using a 300 W halogen lamp box equipped with a band-pass filter (400 nm-700 nm). The intracellular distribution of Alexa 555-labeled CPT/m and late endosomes was assessed at defined time points. Moreover, the colocalization ratio of the fluorescent-labeled CPT/m and late endosomes was quantified by Imaris software (Bitplane, Belfast, United Kingdom).

Blood Circulation of CPT/m Studied by Intravital Microscopy. To study the retention of CPT/m in blood circulation, *in vivo* CLSM was used to observe the blood circulation of CPT/m in live mice. The experiment was performed using a Nikon A1R CLSM installed on an upright ECLIPSE FN1 (Nikon Corp., Tokyo, Japan) and equipped with a 20× objective lens. The pinhole diameter was set to be 10 μm optical slice and a 560 nm diode laser equipped with a band-pass emission filter from 570 to 620 nm was used for tracking Alexa 555-labeled CPT/m. Mice were anesthetized with 2% of isoflurane using a NARCOBIT-E (type II) anesthesia unit (Natsume Seisakusho Co., Ltd., Tokyo, Japan) and maintained in a sedated status. Alexa 555-labeled CPT/m were intravenously injected *via* lateral tail vein, and the fluorescence intensity in the veins and interstitial space of the ear lobe were acquired in video mode by snapshot every 3 s in the first 3 min and then changed to every 1 min. The fluorescence intensity was analyzed by selecting regions of interest (ROI) in vein and extravascular tissues and normalized by comparing with the maximum fluorescence intensity in the vein.

Antitumor Activity of CPT/m against AY27 Xenografts. Balb/c nu/nu mice (6 weeks, 18−20 g) were inoculated subcutaneously with AY27 cancer cells (7.5×10^5 cells/mouse). Tumors were allowed to grow until reaching the average size of 35 mm^3. Subsequently, mice were administered intravenously with PBS, free CPT (5 mg/kg), CPT/m (50 mg/kg on a CPT base) with or without co-injection of Photofrin (2 mg/kg) 3 times with 2-day intervals (days 0, 2 and 4). For the PCI experimental groups, tumors were irradiated (fluence rate, 100 mW/cm^2; time, 10 min) using a xenon lamp equipped with a 610 nm long pass filter (MAX-303, Asahi Spectra, Tokyo, Japan). The antitumor activity was evaluated in terms of tumor volume (V), which was calculated with the following equation:

$$V = (a \times b^2)/2$$

where a represents the major axis and b is the minor axis of the tumor measured by a caliper. The mice were sacrificed at day 14 after intravenous injection when the tumor size of PBS group was over 400 mm^3 and ulceration appeared. The body weight of each mouse was measured as a parameter to evaluate the *in vivo* toxicity.

***In Vivo* Imaging of the PCI of CPT/m.** BALB/c nu/nu mice were subcutaneously inoculated with AY27 cells (7.5×10^5 cells/mouse), and the tumors were allowed to grow until reaching 100 mm^3. Then, the xenograft tumors were surgically exposed, and 10 μL of CellLight Late Endosomes-GFP was dropped on the tumors for late endosomes labeling. Forty-eight hours later, Alexa 555-labeled CPT/m and Photofrin at 2 mg/kg were intravenously injected to the mice, and 24 h later, the *in vivo* CLSM was performed using a Nikon A1R CLSM system equipped with a Apo LWD 40 × /1.15 WI λS objective lens. Before image acquisition, 10 μL of Hoechst 33342 (2 mg/mL in PBS) was dropped on the tumor to stain the nucleus of cells. After that, PCI was induced by irradiating the tumors with a xenon lamp (fluence rate, 100 mW/cm^2; time, 20 s). Snapshots of the tumors were acquired at 0, 1, 3, and 5 h, and the colocalization ratio of Alexa 555-labeled CPT/m with the late endosomes was quantified by Imaris software.

Tumor Accumulation and *in Vivo* PCI-Induced Release of CPT. Balb/c nu/nu mice ($n = 5$) bearing AY27 solid tumors were co-injected with CPT/m at 50 mg/kg on a CPT base and Photofrin at 2 mg/kg. Twenty-four hours later, half of the tumors were irradiated using xenon lamp (fluence rate, 100 mW/cm^2; time, 1000 s). Then, half of the irradiated tumors were collected immediately after irradiation, while the other half were harvested 24 h later. The tumor tissues were homogenized using an ultrasonic homogenizer in PBS buffer. To determine the release ratio of CPT, each tumor was separated into two parts, and one part was treated with DTT to completely release the drug from the micelles. Then, CH_2Cl_2 was used to extract CPT from the homogenates. After evaporation of CH_2Cl_2, the CPT was redissolved in acetonitrile containing 0.5 N HCl, and the concentration was determined by reverse phase liquid chromatography (RPLC) [column, Bondasphere (Waters, Tokyo, Japan); eluent, 1% acetic acid solution/acetonitrile; temperature:, 40 °C; detector, ex, 370 nm; em, 440 nm]. The percentage of released CPT in AY27 tumors was calculated according to the following equation:

$$\%\ \text{of released CPT} = \frac{\text{Free CPT within the tumors}}{\text{Extracted CPT within the tumors treated with DTT}} \times 100$$

***Ex Vivo* CLSM Observation of CPT Release after PCI.** Balb/c nu/nu mice ($n = 5$) bearing AY27 solid tumors were co-injected with CPT/m at 50 mg/kg based on CPT and Photofrin at 2 mg/kg. Twenty-four hours later, half of the tumors were irradiated using a xenon lamp (fluence rate, 100 mW/cm^2; time, 1000 s). Then, half of the irradiated tumors were collected immediately after irradiation, while the other half were harvested 24 h later. All tumors were fixed in 4% paraformaldehyde solution in PBS for 10 min, embedded in optimal cutting temperature (OCT) compound and frozen. Thereafter, tissue sections were sliced using cryostat (Leica CM1950, Leica Biosystems, Wetzlar, Germany) and mounted onto slides for CLSM observation (LSM 510, Carl Zeiss, Oberkochen, Germany). A Mai-Tai two-photon laser set at 730 nm was used as excitation light, and a band-pass filter BP 390−465 was chosen for collecting the fluorescence signal of released CPT in the tumor sections, while fluorescence of CPT inside the micelles remained quenched. The fluorescence intensity was quantified from the images ($n = 30$).

Statistical Analysis. The significance of the results was assessed by Student's t-test. The p-values lower than 0.05 were considered as statistically significant.

Conflict of Interest: The authors declare no competing financial interest.

Supporting Information Available: Additional experimental data as described in text. This material is available free of charge *via* the Internet at http://pubs.acs.org.

Acknowledgment. This study was supported by the Funding Program for World-Leading Innovative R&D on Science and Technology (FIRST Program) from the Japan Society for the Promotion of Science (JSPS), the Center of Innovation (COI), the Program from Japan Science and Technology Agency (JST), the Takeda Science Foundation, Grants-in-Aid for Young Scientists (B; No. 23700526 and No. 25750172 to H.C.; A; No. 24689051 to Y.M.) and Challenging Exploratory Research (No. 24659584 to Y.M.). This study was also partially supported by Initiative for

Accelerating Regulatory Science in Innovative Drug, Medical Device, and Regenerative Medicine (K.K.). AY27 cells were gift from Dr. S. Sato, National Defense Medical College, Saitama, Japan.

REFERENCES AND NOTES

1. Peer, D.; Karp, J. M.; Hong, S.; Farokhzad, O. C.; Margalit, R.; Langer, R. Nanocarriers as an Emerging Platform for Cancer Therapy. *Nat. Nanotechnol.* **2007**, *2*, 751–760.
2. Mura, S.; Nicolas, J.; Couvreur, P. Stimuli-Responsive Nanocarriers for Drug Delivery. *Nat. Mater.* **2013**, *12*, 991–1003.
3. Fleige, E.; Quadir, M. A.; Haag, R. Stimuli-Responsive Polymeric Nanocarriers for the Controlled Transport of Active Compounds: Concepts and Applications. *Adv. Drug Delivery Rev.* **2012**, *64*, 866–884.
4. Lee, Y.; Kataoka, K. Biosignal-Sensitive Polyion Complex Micelles for the Delivery of Biopharmaceuticals. *Soft Matter* **2009**, *5*, 3810–3817.
5. Tong, R.; Kohane, D. S. Shedding Light on Nanomedicine. *WIREs Nanomed. Nanobiotechnol.* **2012**, *4*, 638–662.
6. Fomina, N.; Sankaranarayanan, J.; Almutairi, A. Photochemical Mechanisms of Light-Triggered Release from Nanocarriers. *Adv. Drug Delivery Rev.* **2012**, *64*, 1005–1020.
7. Dowlatshahi, K.; Francescatti, D. S.; Bloom, K. J. Laser Therapy for Small Breast Cancers. *Am. J. Surg.* **2002**, *184*, 359–363.
8. Dolmans, D. E.; Fukumura, D.; Jain, R. K. Photodynamic Therapy for Cancer. *Nat. Rev. Cancer* **2003**, *3*, 380–387.
9. Hogset, A.; Prasmickaite, L.; Selbo, P. K.; Hellum, M.; Engesaeter, B. O.; Bonsted, A.; Berg, K. Photochemical Internalization in Drug and Gene Delivery. *Adv. Drug Delivery Rev.* **2004**, *56*, 95–115.
10. Nishiyama, N.; Iriyama, A.; Jang, W. D.; Miyata, K.; Itaka, K.; Inoue, Y.; Takahashi, H.; Yanagi, Y.; Tamaki, Y.; Koyama, H.; *et al.* Light-Induced Gene Transfer from Packaged DNA Enveloped in a Dendrimeric Photosensitizer. *Nat. Mater.* **2005**, *4*, 934–941.
11. Lai, P. S.; Lou, P. J.; Peng, C. L.; Pai, C. L.; Yen, W. N.; Huang, M. Y.; Young, T. H.; Shieh, M. J. Doxorubicin Delivery by Polyamidoamine Dendrimer Conjugation and Photochemical Internalization for Cancer Therapy. *J. Controlled Release* **2007**, *122*, 39–46.
12. Febvay, S.; Marini, D. M.; Belcher, A. M.; Clapham, D. E. Targeted Cytosolic Delivery of Cell-Impermeable Compounds by Nanoparticle-Mediated, Light-Triggered Endosome Disruption. *Nano Lett.* **2010**, *10*, 2211–2219.
13. Lu, H. L.; Syu, W. J.; Nishiyama, N.; Kataoka, K.; Lai, P. S. Dendrimer Phthalocyanine-Encapsulated Polymeric Micelle-Mediated Photochemical Internalization Extends the Efficacy of Photodynamic Therapy and Overcomes Drug-Resistance *In Vivo*. *J. Controlled Release* **2011**, *155*, 458–464.
14. Nomoto, T.; Fukushima, S.; Kumagai, M.; Machitani, K.; Arnida; Matsumoto, Y.; Oba, M.; Miyata, K.; Osada, K.; Nishiyama, N.; *et al.* Three-Layered Polyplex Micelle as a Multifunctional Nanocarrier Platform for Light-Induced Systemic Gene Transfer. *Nat. Commun.* **2014**, *5*, No. 3545.
15. Pasparakis, G.; Manouras, T.; Vamvakaki, M.; Argitis, P. Harnessing Photochemical Internalization with Dual Degradable Nanoparticles for Combinatorial Photo-Chemotherapy. *Nat. Commun.* **2014**, *5*, No. 3623.
16. Kataoka, K.; Harada, A.; Nagasaki, Y. Block Copolymer Micelles for Drug Delivery: Design, Characterization and Biological Significance. *Adv. Drug Delivery Rev.* **2001**, *47*, 113–131.
17. Nishiyama, N.; Kataoka, K. Current State, Achievements, and Future Prospects of Polymeric Micelles as Nanocarriers for Drug and Gene Delivery. *Pharmacol. Ther.* **2006**, *112*, 630–648.
18. Cabral, H.; Kataoka, K. Progress of Drug-Loaded Polymeric Micelles into Clinical Studies. *J. Controlled Release* **2014**, *190*, 465–476.
19. Kakizawa, Y.; Harada, A.; Kataoka, K. Environment-Sensitive Stabilization of Core−Shell Structured Polyion Complex Micelle by Reversible Cross-Linking of the Core through Disulfide Bond. *J. Am. Chem. Soc.* **1999**, *121*, 11247–11248.
20. Miyata, K.; Kakizawa, Y.; Nishiyama, N.; Harada, A.; Yamasaki, Y.; Koyama, H.; Kataoka, K. Block Catiomer Polyplexes with Regulated Densities of Charge and Disulfide Cross-Linking Directed to Enhance Gene Expression. *J. Am. Chem. Soc.* **2004**, *126*, 2355–2361.
21. Cabral, H.; Nakanishi, M.; Kumagai, M.; Jang, W. D.; Nishiyama, N.; Kataoka, K. A Photo-Activated Targeting Chemotherapy Using Glutathione Sensitive Camptothecin-Loaded Polymeric Micelles. *Pharm. Res.* **2009**, *26*, 82–92.
22. Schafer, F. Q.; Buettner, G. R. Redox Environment of the Cell as Viewed through the Redox State of the Glutathione Disulfide/Glutathione Couple. *Free Radical Biol. Med.* **2001**, *30*, 1191–1212.
23. Austin, C. D.; Wen, X.; Gazzard, L.; Nelson, C.; Scheller, R. H.; Scales, S. J. Oxidizing Potential of Endosomes and Lysosomes Limits Intracellular Cleavage of Disulfide-Based Antibody-Drug Conjugates. *Proc. Natl. Acad. Sci. U.S.A.* **2005**, *102*, 17987–17992.
24. Huang, Z. A Review of Progress in Clinical Photodynamic Therapy. *Technol. Cancer Res. Treat.* **2005**, *4*, 283–293.
25. Prasmickaite, L.; Høgset, A.; Berg, K. Evaluation of Different Photosensitizers for Use in Photochemical Gene Transfection. *Photochem. Photobiol.* **2001**, *73*, 388–395.
26. Walther, M. M.; Delaney, T. F.; Smith, P. D.; Friauf, W. S.; Thomas, G. F.; Shawker, T. H.; Vargas, M. P.; Choyke, P. L.; Linehan, W. M.; Abraham, E. H.; *et al.* A Phase I Trial of Photodynamic Therapy in the Treatment of Recurrent Superficial Transition Cell Carcinoma of the Bladder. *Urology* **1997**, *50*, 199–206.
27. Osada, K.; Shiotani, T.; Tockary, T. A.; Kobayashi, D.; Oshima, H.; Ikeda, S.; Christie, R. J.; Itaka, K.; Kataoka, K. Enhanced Gene Expression Promoted by the Quantized Folding of pDNA within Polyplex Micelles. *Biomaterials* **2012**, *33*, 325–332.
28. Harada, A.; Kataoka, K. Novel Polyion Complex Micelles Entrapping Enzyme Molecules in the Core. 2. Characterization of the Micelles Prepared at Nonstoichiometric Mixing Ratios. *Langmuir* **1999**, *15*, 4208–4212.
29. Tockary, T. A.; Osada, K.; Chen, Q.; Machitani, K.; Dirisala, A.; Uchida, S.; Nomoto, T.; Toh, K.; Matsumoto, Y.; Itaka, K.; *et al.* Tethered PEG Crowdedness Determining Shape and Blood Circulation Profile of Polyplex Micelle Gene Carriers. *Macromolecules* **2013**, *46*, 6585–6592.
30. Mochida, Y.; Cabral, H.; Miura, Y.; Albertini, F.; Fukushima, S.; Osada, K.; Nishiyama, N.; Kataoka, K. Bundled Assembly of Helical Nanostructures in Polymeric Micelles Loaded with Platinum Drugs Enhancing Therapeutic Efficiency against Pancreatic Tumor. *ACS Nano* **2014**, *8*, 6724–6738.
31. Yamamoto, Y.; Nagasaki, Y.; Kato, Y.; Sugiyama, Y.; Kataoka, K. Long-Circulating Poly(Ethylene Glycol)-Poly(D,L-Lactide) Block Copolymer Micelles with Modulated Surface Charge. *J. Controlled Release* **2001**, *77*, 27–38.
32. Matsumura, Y.; Maeda, H. A New Concept for Macromolecular Therapeutics in Cancer Chemotherapy: Mechanism of Tumoritropic Accumulation of Proteins and the Antitumor Agent Smancs. *Cancer Res.* **1986**, *46*, 6387–6392.
33. Matsumoto, Y.; Nomoto, T.; Cabral, H.; Matsumoto, Y.; Watanabe, S.; Christie, R. J.; Miyata, K.; Oba, M.; Ogura, T.; Yamasaki, Y.; *et al.* Direct and Instantaneous Observation of Intravenously Injected Substances Using Intravital Confocal Micro-Videography. *Biomed. Optics Express* **2010**, *1*, 1209–1216.
34. Hamaguchi, T.; Matsumura, Y.; Suzuki, M.; Shimizu, K.; Goda, R.; Nakamura, I.; Nakatomi, I.; Yokoyama, M.; Kataoka, K.; Kakizoe, T. NK105, a Paclitaxel-Incorporating Micellar Nanoparticle Formulation, Can Extend *in Vivo* Antitumour Activity and Reduce the Neurotoxicity of Paclitaxel. *Br. J. Cancer* **2005**, *92*, 1240–1246.
35. Nishiyama, N.; Okazaki, S.; Cabral, H.; Miyamoto, M.; Kato, Y.; Sugiyama, Y.; Nishio, K.; Matsumura, Y.; Kataoka, K. Novel Cisplatin-Incorporated Polymeric Micelles Can Eradicate Solid Tumors in Mice. *Cancer Res.* **2003**, *63*, 8977–8983.
36. Cabral, H.; Matsumoto, Y.; Mizuno, K.; Chen, Q.; Murakami, M.; Kimura, M.; Terada, Y.; Kano, M. R.; Miyazono, K.;

Uesaka, M.; *et al.* Accumulation of Sub-100 nm Polymeric Micelles in Poorly Permeable Tumours Depends on Size. *Nat. Nanotechnol.* **2011**, *6*, 815–823.
37. Beretta, G. L.; Zunino, F. Relevance of Extracellular and Intracellular Interactions of Camptothecins as Determinants of Antitumor Activity. *Biochem. Pharmacol.* **2007**, *74*, 1437–1444.
38. Miyazaki, K.; Morimoto, Y.; Nishiyama, N.; Maekawa, Y.; Hu, W. Z.; Nakatate, K.; Kaneda, K.; Shinomiya, N.; Kataoka, K. A Novel Homogeneous Irradiation Fiber Probe for Whole Bladder Wall Photodynamic Therapy. *Lasers Surg. Med.* **2012**, *44*, 413–420.
39. Miyazaki, K.; Morimoto, Y.; Nishiyama, N.; Satoh, H.; Tanaka, M.; Shinomiya, N.; Ito, K. Preconditioning Methods Influence Tumor Property in an Orthotopic Bladder Urothelial Carcinoma Rat Model. *Mol. Clin. Oncol.* **2014**, *2*, 65–70.
40. Kim, H.; Lee, D.; Kim, J.; Kim, T. I.; Kim, W. J. Photothermally Triggered Cytosolic Drug Delivery *via* Endosome Disruption Using a Functionalized Reduced Graphene Oxide. *ACS Nano* **2013**, *7*, 6735–6746.
41. Li, Y. S.; Reid, C. N.; McHale, A. P. Enhancing Ultrasound-Mediated Cell Membrane Permeabilisation (Sonoporation) Using a High Frequency Pulse Regime and Implications for Ultrasound-Aided Cancer Chemotherapy. *Cancer Lett.* **2008**, *266*, 156–162.
42. Domenech, M.; Marrero-Berrios, I.; Torres-Lugo, M.; Rinaldi, C. Lysosomal Membrane Permeabilization by Targeted Magnetic Nanoparticles in Alternating Magnetic Fields. *ACS Nano* **2013**, *7*, 5091–5101.
43. Daly, W. H.; Poché, D. The Preparation of *N*-Carboxyanhydrides of α-Amino Acids Using Bis(trichloromethyl) Carbonate. *Tetrahedron Lett.* **1988**, *29*, 5859–5862.
44. Aitken, A.; Learmonth, M. Estimation of Disulfide Bonds Using Ellman's Reagent. In *The Protein Protocols Handbook*; Walker, J. M., Ed.; Springer: New York, 1996; pp 1053−1055.